## A simple experimental setup to demonstrate the basics of positron emission tomography

Kerstin Sonnabend, Wolfgang Bayer, Peter Mohr, and Andreas Zilges

Citation: American Journal of Physics 70, 929 (2002);

View online: https://doi.org/10.1119/1.1488636

View Table of Contents: http://aapt.scitation.org/toc/ajp/70/9 Published by the American Association of Physics Teachers

#### Articles you may be interested in

A simple medical physics experiment based on a laser pointer American Journal of Physics **70**, 1068 (2002); 10.1119/1.1488640

A simple electron-positron pair production experiment

American Journal of Physics 74, 457 (2006); 10.1119/1.2174030

From Lorenz to Coulomb and other explicit gauge transformations

American Journal of Physics 70, 917 (2002); 10.1119/1.1491265

Entangled photon apparatus for the undergraduate laboratory

American Journal of Physics 70, 898 (2002); 10.1119/1.1498859

Polar and axial vectors versus quaternions

American Journal of Physics 70, 958 (2002); 10.1119/1.1475326

An algebraic method for solving central force problems

American Journal of Physics 70, 945 (2002); 10.1119/1.1491262



# A simple experimental setup to demonstrate the basics of positron emission tomography

Kerstin Sonnabend, <sup>a)</sup> Wolfgang Bayer, Peter Mohr, and Andreas Zilges Institut für Kernphysik, TU Darmstadt, Schlossgartenstrasse 9, 64289 Darmstadt, Germany

(Received 21 June 2001; accepted 2 May 2002)

We present a setup of a simplified positron emission tomograph (PET) which can be used in a third-year laboratory course for physics students. The equipment of a standard  $\gamma-\gamma$  angular correlation experiment was modified using bismuth-germanate crystals instead of NaI. Using this setup it is possible to locate several radioactive sources hidden in a closed box. The problems of two-dimensional imaging tomography using one-dimensional projections are illustrated as well as the problems encountered in medical PET examinations. © 2002 American Association of Physics Teachers. [DOI: 10.1119/1.1488636]

#### I. INTRODUCTION

Positron emission tomography (PET), magnetic resonance imaging (MRI), and computerized tomography (CT or CAT) are some of the most rapidly developing diagnostic imaging procedures in modern medicine. Classical x-ray images and CT both probe static tissue properties using the variation of x-ray absorption in different tissues. Hence, these images can be used to distinguish between bones and other tissue to observe damaged bones.

In contrast to x-ray absorption, MRI images are a consequence of the concentration of hydrogen stored naturally in the body and the character of its surroundings. Thus, MRI results in less radiation exposure to the organism. PET uses instead the localization of radioactive tracers. Hence, PET images depict how much of the chemical compound carrying the tracer is consumed in the observed area, that is, the physiological activity belonging to the chemical compound is pictured. Therefore, PET images are called physiological. Many diseases such as cancer, heart diseases, and disorders of the brain can be diagnosed at a very early stage using physiological images to complement anatomical information.

The idea of PET is to use the two collinear photons emitted following the annihilation of a positron. If the energy of the positron is close to the binding energy of atomic electrons (several electron volts), it annihilates by emission of two back-to-back photons with  $E_{\gamma}$ =511 keV corresponding to the rest masses of the electron and positron. The maximum kinetic energy of a positron after a  $\beta^+$  decay is typically around 1 MeV, giving the positron a range of between 0.5 and 2 mm in human tissue before annihilation takes place. The entire process is schematically depicted in Fig. 1.

In a PET tomograph, the detectors are coupled electronically to several pairs, each pair observing a line of response (LOR). If both detectors measure an event in a fixed time window (usually about 15 ns<sup>1</sup>), an annihilation has taken place at the LOR. Due to the known angular correlation between annihilation photons, the spatial resolution is not enhanced using collimators like in Anger cameras. Thus, the principle of PET is known as a self-collimating one.

The position resolution of PET images is limited by several physical effects. The positron range is the dominating limit for the spatial resolution. In addition, the detector size limits the precise determination of the position of the annihilation. Smaller sources of uncertainty are caused by the error in collinearity of the emitted photons because of the

residual energy of the two particles. Accidental coincidences can be minimized by using a short coincidence-resolving time while suppression of scattering events requires detectors with good energy resolution and an adequate determination of thresholds of the electronic components (see Ref. 1).

Although the first attempts to build a PET system were made in the early 1960s, <sup>1</sup> the first industrial PET scanners arrived only in 1975 because of the extremely time-consuming reconstruction algorithms and the special requirements of the radioactive tracers. The availability of adequate tracers is still a special problem of PET while the search for accurate reconstruction algorithms is of common interest to many imaging methods including those mentioned above.<sup>2</sup>

The tracers used for PET must be labeled with positronemitting isotopes. The lifetime of the isotopes has to be longer than the time needed for production and measurement (including separation of the radionuclides, chemical processing, and application to the patient). However, to avoid long measuring times and high radioactive doses for the patient, lifetimes of more than 2 h are not practical. The most important PET isotopes for medical imaging are listed in Table I as well as <sup>22</sup>Na, which we have chosen for practical reasons in our student lab.

Although in the early days PET was mainly used to study the functionality of the brain, today whole-body scans are used, for example, to unmask cancer cells by their abnormal metabolism of glucose. The spatial localization of a tracer is often useful in other scientific fields as well. For example, psychologists use PET images to distinguish the different functional regions of the brain. New applications are continuously being developed (for further information see Refs. 1 and 3 and collected editions such as Refs. 4–8).

Although the commercial realization of PET is difficult, the principles and problems of using this technique can be taught to students by going back to basic physics. Only two detectors are necessary to measure two photons in coincidence. A large number of detectors mainly reduces the measuring time because many LORs can be detected simultaneously. The necessity to measure as many LORs as possible can be derived from the central slide theorem—the basis for the reconstruction of two-dimensional pictures from parallel projections—which was first proposed by Radon in 1917. Let  $\phi$  be the angle of the observation direction in the (x,y) plane and s the belonging position vector. Then define  $p(s,\phi)$  to be the parallel projection of the two-dimensional function f(x,y) at an angle  $\phi$ . The basic idea of the central

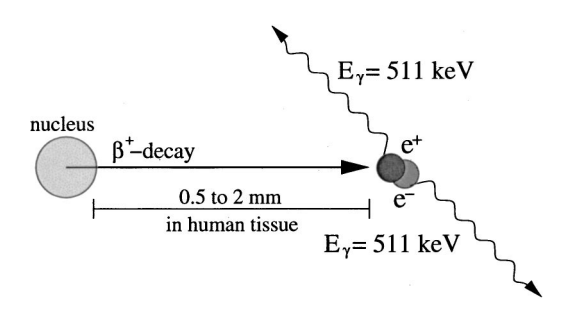


Fig. 1.  $\beta^+$  decay and annihilation of the positron. The typical range of the positrons emitted by medical tracers is between 0.5 and 2 mm in human tissue (compare Table I). This is the physical limit of spatial resolution for PET imaging. The error for the collinearity is about  $0.5^{\circ}$  due to the residual energy of positron and electron.

slide theorem is that the one-dimensional Fourier transform of  $p(s,\phi)$  is exactly the two-dimensional Fourier transform of f(x,y) at an angle  $\phi$ . Therefore, f(x,y) can be recovered from the Fourier transforms of the complete set, that is, the continuous distribution of one-dimensional parallel projections,  $p(s,\phi)$  as a function of  $\phi$ .

However, in reality a continuous distribution will never be realized, and thus the Fourier reconstruction is incorrect (for example, the reconstructed picture of a point is a broadened spot). Sampling projections for a satisfactory reconstruction with our simplified setup would take much more time than available in a course. That is why we have developed a simple reconstruction algorithm for our special experimental situation.

The experimental setup and its construction is described in Sec. II, and the performance of the setup and our reconstruction algorithm are discussed in Sec. III. Section IV describes how the setup is used in the lab and which problems the students have to solve. Finally Sec. V summarizes our experiences with the setup and presents several ideas for its further use and improvement. A list of the detectors, radioactive sources, and electronic components is presented in the Appendix.

#### II. SETUP OF THE EXPERIMENT

The first step of a PET examination is the injection of a radioactive tracer in the patient's body. The glucose analog FDG [(<sup>18</sup>F)2-deoxy-2-fluoro-D-glucose] is used commonly to examine physiological processes like glucose metabolism. Other tracers must be chosen for other needs such as the investigation of oxygen metabolism or the tracing of medications. After some time, the patient is positioned inside the PET scanner.

Commercial PET scanners found in medical centers consist of several rings of scintillation detectors. Each of these

Table I. Lifetimes of the four most important PET isotopes and <sup>22</sup>Na.

Isotope	$T_{1/2}$	$E_{\max}(\beta^+)$ (MeV)	Eff range (mm)	Typ prod reaction	Other $\gamma$ 's
<sup>11</sup> C	20.3 min	0.97	2.06	$^{14}N(p,\alpha)^{11}C$	
$^{13}N$	10.0 min	1.19	3	$^{16}O(p,\alpha)^{13}N$	• • •
<sup>15</sup> O	124 s	1.7	4.5	$^{14}N(d,n)^{15}O$	
$^{18}$ F	110 min	0.635	1.4	$^{18}{\rm O}(p,n)^{18}{\rm F}$	• • • •
<sup>22</sup> Na	2.6 yr	0.5	•••	$^{24}{ m Mg}(d,lpha)^{22}{ m Na}$	1275 keV

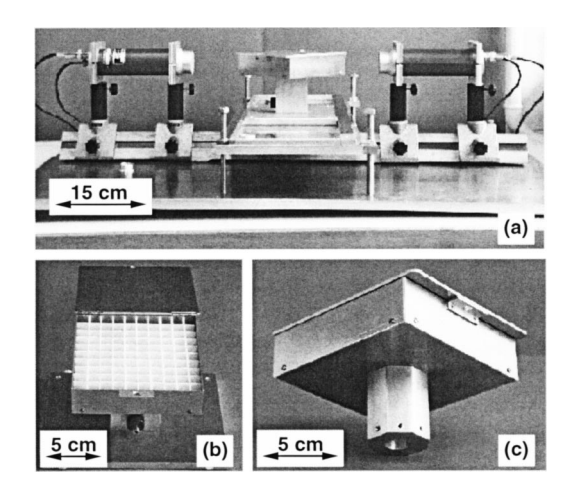


Fig. 2. (a) Overview of the mechanical setup. The sled with the box is surrounded by the two BGO detectors on the left and right. The sled can be moved on a track perpendicular to the LOR of the detectors. (b) The box with its inlay made of polystyrol. (c) The eight-cornered shaft of the box. This shape allows the box to be fixed at  $0^{\circ}$ ,  $45^{\circ}$ , and  $90^{\circ}$  with respect to the LOR.

rings contains 512 or more detectors which are read in coincidence with detectors of the same or neighboring rings. Therefore many LORs are measured simultaneously, and the recorded data are used to calculate pictures of the distribution of the radioactive tracer in the patient's tissue.

The basics of the PET method, the coincident measuring of two back-to-back photons, can be shown using two detectors counting the events caused by a pointlike positron emitter like  $^{22}$ Na. The position of the source in a two-dimensional grid is determined with a simple reconstruction procedure as explained in Sec. III. Such a setup can be realized by minor modifications of a standard experiment used to measure  $\gamma$ – $\gamma$  angular correlations (see Refs. 10 and 11).

The mechanical setup is optimized to measure projections of the distribution of radioactivity in a closed box. For this purpose, the box is fixed on an eight-cornered shaft [see Fig. 2(c)] allowing us to measure projections at angles of 0°, 45°, and 90°. Once an angle is chosen, the box has to be moved perpendicular to the LOR of the detectors. Therefore, the shaft of the box is put into a square tube which is fixed on a plate. This sled can be moved on a track where its position is determined with a ruler. To change the geometrical efficiency of the setup, the distance between the detectors can be chosen by shifting them on a rail. The rail and the track are both positioned on a thick plate which can be leveled.

Figure 2(a) depicts an overview of the setup with the two detectors on the left and right. Most of the described mechanical setup is made of aluminum because of its excellent manufacturing properties. However, the grid inside the box [see Fig. 2(b)] has to be made of a different material with low absorption coefficient in order to reduce  $\gamma$ -ray absorption. We choose polystyrol with an absorption coefficient of  $\mu = (0.085 \pm 0.002) \, \mathrm{cm}^{-1}$ .

The detectors used for the setup are bismuth-germanate crystals (Bi $_4$ Ge $_3$ O $_{12}$  or BGO), with a size of 30 mm  $\times$ 20 mm (diameter $\times$ height). BGO crystals are the standard scintillation material in commercial PET scanners because the high density of BGO ( $\rho_{BGO}$ =7.13 g/cm $^3$ ) and the large atomic number of the bismuth component ( $Z_{Bi}$ =83) yields a

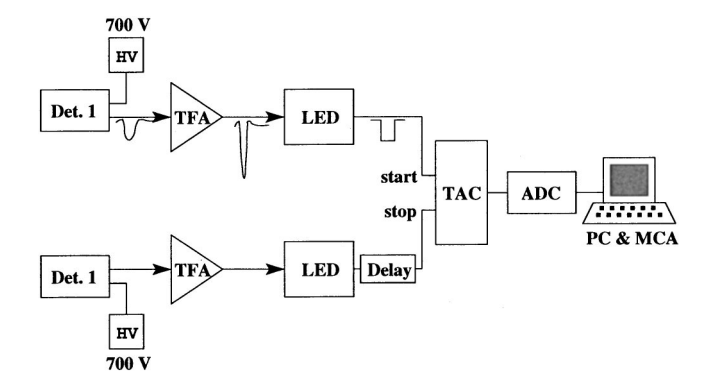


Fig. 3. The electronic setup. The detectors require a high voltage supply of 700 V. Each detector output is shaped and amplified by a timing filter amplifier and converted to a logical signal by a leading edge discriminator. The timing spectrum, which is displayed on a standard personal computer, is created by the resulting time-to-amplitude converter output that is digitalized by an analog-to-digital converter.

higher probability per unit volume for the photoelectric effect than that of NaI ( $\rho_{NaI}$ =3.67 g/cm<sup>3</sup>,  $Z_{I}$ =53).<sup>12</sup>

The electronic setup is based on standard  $\gamma - \gamma$  angular correlation techniques (see Fig. 3 and Refs. 10 and 11). The signal from each photomultiplier is amplified and shaped by one of the timing filter amplifiers. 13 The rise time is reduced from about 0.3 µs to a few nanoseconds. If the height of the timing filter amplifier output signal exceeds the adjustable threshold of the leading edge discriminator, a logic signal is obtained. One of these signals is used to start a time-toamplitude converter while the other one, after passing a delay, stops it. Hence, the time-to-amplitude converter output signal carries information on the time difference between the advent of two annihilation quanta in the two detectors. The program WINTMCA<sup>14</sup> is used to display the time spectra. The required digital input is created by an analog-to-digital converter and a multichannel analyzer which is installed in a personal computer.

#### III. PERFORMANCE OF THE SETUP

The setup described in Sec. II allows measurements which are also relevant for industrial PET scanners. The first is the calibration of timing using different delays between start and stop signals of the time-to-amplitude converter. Figure 4

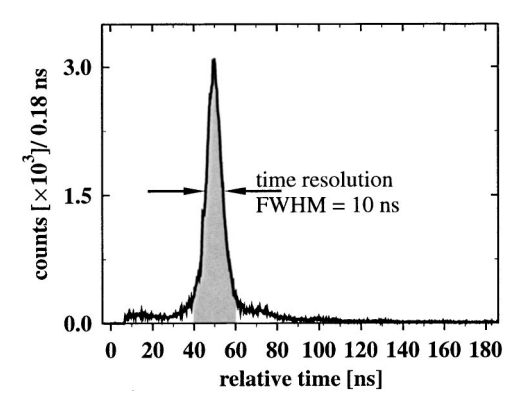


Fig. 4. The timing spectrum between the two BGO detectors. The time resolution is determined from the FWHM of the peak, which is better than 10 ns. The grey-shaded area is integrated and taken as a measure for the number of coincident events.

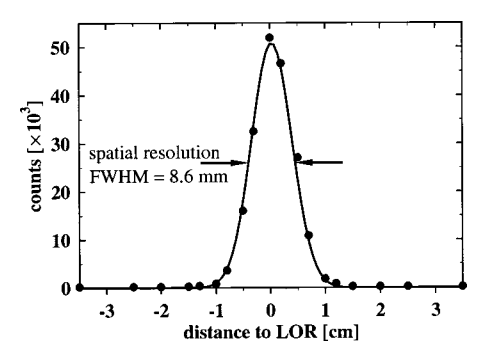


Fig. 5. Example of the spatial resolution using the self-collimating principle of PET. To determine the spatial resolution the source is placed at different distances relative to the LOR of the detectors. The number of coincident events is plotted for each distance chosen. The error of the measured points is smaller than the size of the dots. The line is a Gaussian fit to the data with FWHM of about 8.6 mm. One can see that the position of the source is determined with an error of less than 2 mm.

shows the result of a calibration—the time resolution of our setup is better than 10 ns. The peak in the spectrum is integrated over a range of  $\Delta t = 23$  ns to determine the number of coincident events.

The spatial resolution is measured by placing the source at different distances to the LOR. Two pairs of collimators can be mounted in front of the BGO detectors to find the optimum results. Using the broader collimators yields a spatial resolution of 8.6 mm at full width at half maximum (FWHM). Choosing the smaller collimators has almost no influence on the spatial resolution because of the self-collimating principle of PET. Figure 5 shows that the distance of the source to the LOR is determined with an accuracy better than 2 mm.

To simulate a PET examination, the box with the grid inside is loaded with two (or more) radioactive point sources of different activities. The box is closed and the students have to find the positions of the sources. For that purpose the matrix of the distribution of radioactivity in the observed area is calculated using the number of coincident events at different positions for two directions of projection.

The left part of Fig. 6 explains this procedure: If there are n projections in direction x and m projections in direction y, then there are  $m \times n$  crossing points. The value  $A_{xy}(i,j)$  of each crossing point with coordinates (i,j) is calculated from the measured intensities  $A_x(i)$  and  $A_y(j)$   $(i \in [1,n], j \times \in [1,m])$ ,

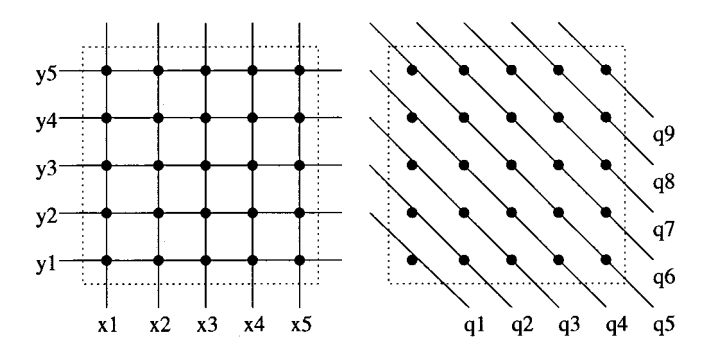


Fig. 6. Calculation of the two-dimensional distribution. The left-hand side explains the calculation of the distribution using five projections in both x and y directions. The right-hand side shows the projections in the third direction indicated by q.

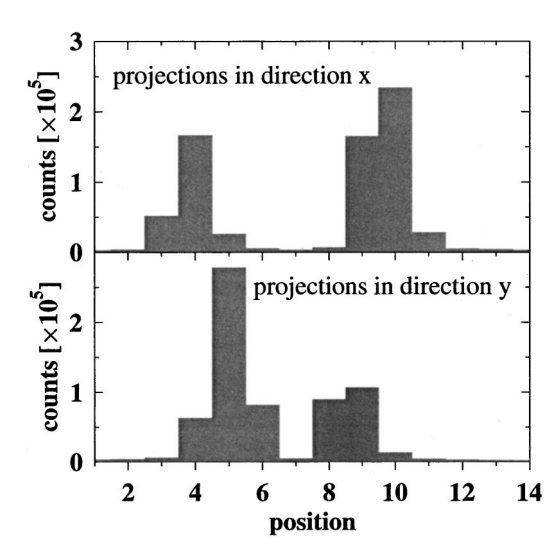


Fig. 7. Results of the scanning of the box in 14 steps per direction. The distance between two projections was 10 mm. The upper part presents the coincident counting rates of different projections in the x direction, and the lower one in the y direction. The values were determined by integrating the peak of the dedicated timing spectrum (compare Fig. 4).

$$A_{xy}(i,j) = A_x(i)A_y(j). \tag{1}$$

Figure 7 shows an example of the measured activity in the two directions. In this example, 14 projections per direction were measured for 5 min, which yielded a relative statistical error  $\Delta A_x(i)/A_x(i)$  of about 0.2% at maximum intensity. The calculated two-dimensional distribution is shown in Fig. 8. The picture seems to indicate the existence of four sources, although only two sources have been placed in the box. The reason for these artifacts is the reconstruction procedure: Two sources result in two points of high activity in each direction of projection. Multiplying the values yields four crossing points of high activity in the calculated two-dimensional intensity distribution.

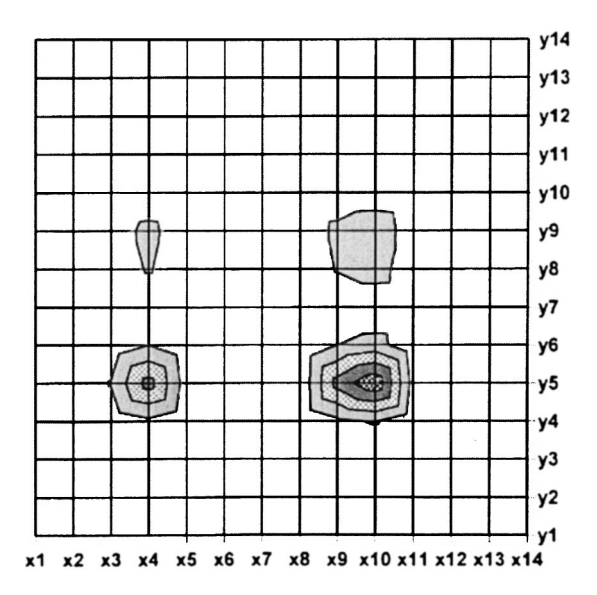


Fig. 8. Distribution of coincident counting rate calculated using the projections in the x and y directions. The grey scale represents the calculated intensity  $A_{xy}(i,j)$ . Four regions of high activity can be seen, although there were only two sources near the positions  $(x_4, y_9)$  and  $(x_{10}, y_5)$ .

A similar problem occurs also in the use of "real" tomographs. Although hundreds of LORs are measured simultaneously, a finite number of detectors can still cause artifacts in the reconstructed image when using Fourier transformation algorithms.

To avoid these problems in real PET examinations, the filtered backprojection or the iterative reconstruction methods can be used. The filtered backprojection method rejects all frequencies in the Fourier space without useful information. Iterative reconstruction compares the theoretical distributions and their reconstruction with the results. The theoretical assumption is correct when satisfactory agreement is reached.

In the simple case of only two sources, it is fortunately sufficient to refine the reconstruction procedure in order to measure the correct number and positions of the hidden sources. The easiest possibility is to measure further projections in a third direction and to multiply these new results by the former matrix.

The right part of Fig. 6 shows that (n+m-1) projections in the third direction are needed to reach every crossing point of the preceding matrix. We can also calculate the new distance between the projections in this direction—the q or diagonal direction. If  $\Delta x$  is the distance in the x direction and  $\Delta y$  that in the y direction, we obtain

$$\Delta q = \frac{\sqrt{\Delta x^2 + \Delta y^2}}{2}. (2)$$

The new value of the crossing point with index (i,j),  $A_{xyq}(i,j,k)$ , is calculated using the measured intensity  $A_{q}(k)$ ,

$$A_{xyq}(i,j,k) = A_q(k)A_{xy}(i,j).$$
 (3)

The correlation between the indices is

$$k = i + j - 1, \tag{4}$$

with  $k \in [1, n+m-1]$ .

Why does multiplication by the third intensity  $A_q(k)$  result in a rejection of the artifacts? Let us assume that we have two point sources located at the crossing points (i,k) and (j,l). Using the x and y directions results in local maxima at  $A_{xy}(i,k)$ ,  $A_{xy}(i,l)$ ,  $A_{xy}(j,k)$ , and  $A_{xy}(j,l)$ . If direction q is also measured, high values are obtained only for  $A_q(i+k-1)$  and  $A_q(j+l-1)$ , but not for  $A_q(i+l-1)$  and  $A_q(j+k-1)$  which belong to the artifacts. Therefore, the new calculated values  $A_{xyq}$  will always mirror the real situation.

The information found from the diagonal direction measurement is shown in Fig. 9. If the counts are multiplied by the crossing points of Fig. 8, we obtain the corrected intensity matrix shown in Fig. 10. Using Fig. 10 the locations of the sources in the box can be determined without ambiguity.

If more than two sources are hidden in the box, we need more than three directions of projection. One can show that the number of directions needed,  $N_{\rm dir}$ , increases with the number of hidden point sources,  $N_{\rm source}$ , as

$$N_{\rm dir} = N_{\rm source} + 1. \tag{5}$$

Our reconstruction method is obviously only practical for a small number of point sources. For the special conditions of our experimental setup our method is both less time-consuming and mathematically easier than the reconstruction using the central slide theorem. <sup>9</sup> Nevertheless, the problem

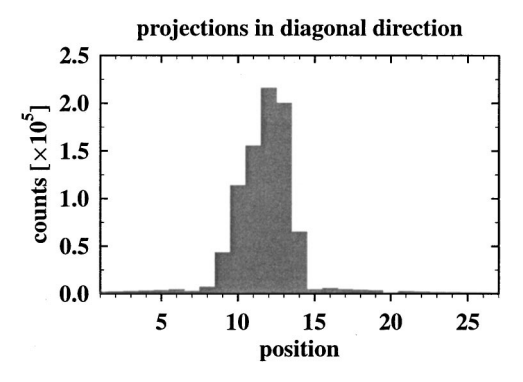


Fig. 9. Result of the scanning of the box in the diagonal direction; 27 projections were measured with a distance  $\Delta q$  of  $\approx$  7.1 mm [calculated using Eq. (2)].

of artifacts is illustrated in a very simple and obvious way.

After determining the locations of the radioactive sources, the ratio of the activities of the hidden point sources can be calculated. The simplest way is to use the maximum values of the different peaks in the direction of projection in which their separation is greatest. The ratio of the values yields a good approximation to the real activity ratio which in our case was one to two (compare Fig. 7). To improve the calculation, different positions of the sources at the LOR and thereby different geometrical cross sections  $\epsilon_{\rm geo}$  must be considered.

#### IV. PRACTICAL TRAINING OF STUDENTS

The setup described in this paper is used in the laboratory course for physics students in their third year. They have to solve different problems with the aim being not only to teach them the basics of PET, but also the principle of coincident measurements and the general problems of constructing two-dimensional pictures using one-dimensional projections.

At the beginning of the lab students measure the energy spectrum of <sup>22</sup>Na, which should be a familiar task, and dis-

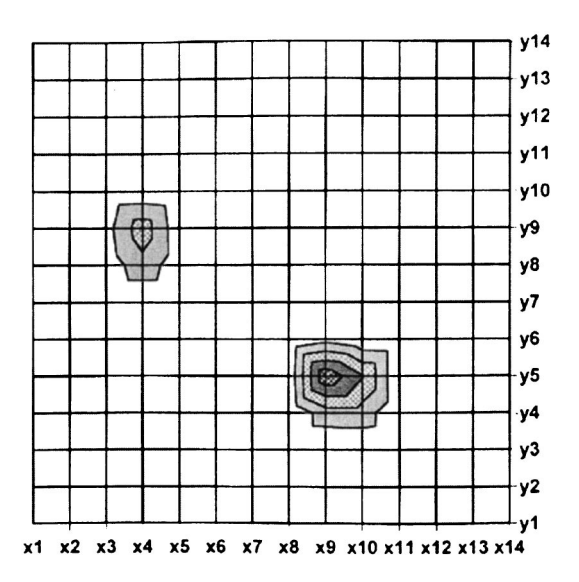


Fig. 10. Corrected distribution of coincident counting rate. The grey scale represents the calculated intensity  $A_{xyq}(i,j,k)$ . Only two regions of high activity remain. A comparison with Fig. 8 shows that the x value of the stronger source is moved one unit to the left belonging to the superposition of the sources in the diagonal direction.

cuss whether this source is a good choice for a PET simulation. The electronic circuit shown in Fig. 3 is constructed by the students on their own. After adding new components the output has to be checked and interpreted using an oscilloscope. Thresholds, delays, amplification, etc., have to be adjusted if necessary. In this way, the students become aquainted with these standard electronic components and their interplay.

Then the time and spatial resolution are measured as described in Sec. III. To allow a more student-centered experiment, the students must find and argue for their favorite combination of parameters such as the time of measurement, the distance between the projections, and the use of collimators. Many of these combinations yield an acceptable result in the PET simulation which was described in detail in Sec. III. The evaluation of the data includes the determination of the position of the hidden sources and of the ratio of their activities. The difficulty of artifacts and their prevention should be discussed as well. After the evaluation of their data, the students have to reflect upon their choice of parameters and discuss probable error sources. Thereby, they gain insight into the principle and difficulties of PET and also learn about the general steps involved in planning and evaluating an experiment.

#### V. CONCLUSION AND OUTLOOK

The experiment has been offered for two years. The student response has been enthusiastic because of greater student involvement in some of the details of the experiment and the direct relation to practical applications. Participants praise the general idea of planning and executing an experiment on their own, including the evaluation of the data and the interpretation of the results. Instructors are impressed by the different problem-solving strategies used by the students.

We are convinced that the same setup could be used in medical lab courses as well, so that medical students could become acquainted with the physical basis of a diagnostic imaging procedure and the problems of reconstruction.

There are several ways to extend the experiment both in terms of the setup and the lessons. The former includes the simulation of special cases of PET examinations, for example, 3D-PET or time of flight-PET. A further lesson using the present setup is the determination of the absolute values of the activities of the sources, while another interesting lesson, especially if medical students are involved, would be the comparison of PET and single photon emission computed tomography which can also be realized with the present setup.

#### **APPENDIX**

List of electronic components (similar EG&G ORTEC modular electronic instruments are given in brackets).

Detectors: Scionix Holland BV dedicated scintillation detectors consisting of a BGO crystal, dimensions 30 mm  $\times 20$  mm, coupled to a photomultiplier tube type Hamamatsu 2060 with integrated voltage divider, mounted in an aluminum housing.

High voltage supply: ORTEC model 556 high voltage power supply, 0–3000 V, 0–10 mA.

Timing filter amplifier: ORTEC model 474.

Leading edge discriminator: LeCroy model 821 (two ORTEC model 473A).

Delay: self-made, 2.5-66 ns (ORTEC model 425A).

Time-to-amplitude converter: EMI/NE (Nuclear Enterprises), time converter (no longer available); range  $0.05-10~\mu s$  (ORTEC model 457).

Analog-to-digital converter: Montedel, 8192 ADC model 8215.

Multichannel analyzer: target, TMCA2-02 card for WinTMCA.

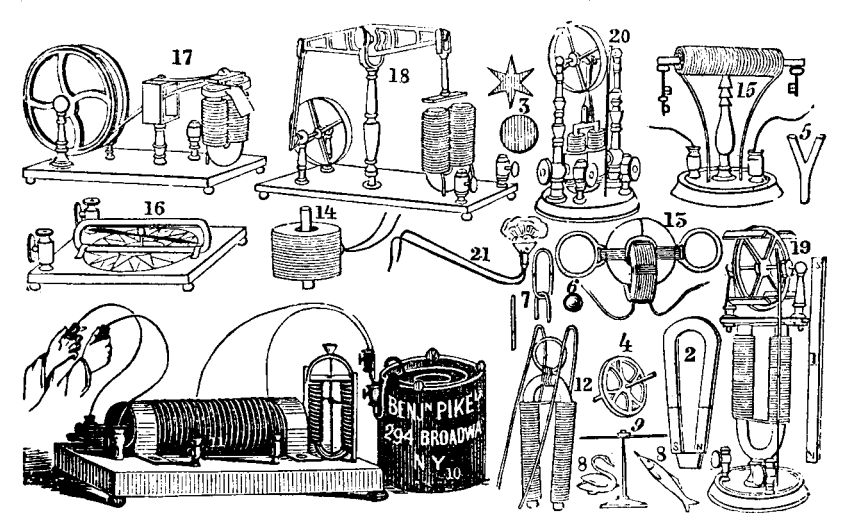
Radioactive sources: two  $^{22}$ Na calibration sources with different activities,  $A_1 = 211$  kBq,  $A_2 = 430$  kBq.

Mechanical setup: the CAD sketches can be requested from Wolfgang Bayer at TU Darmstadt, Germany, bayer@ikp.tu-darmstadt.de.

If there are further questions about the setup or the procedure of the experiment, please contact Kerstin Sonnabend at TU Darmstadt, Germany, kerstin@ikp.tu-darmstadt.de.

- <sup>2</sup>See, for example, the many articles on image reconstruction in IEEE Trans. Med. Imag.
- <sup>3</sup>U. Pietrzyk, *Positron Emission Tomography—Physical Background and Applications* (Shaker Verlag GmbH, Berlin, 1999).
- <sup>4</sup>H. J. Wieler, PET in Clinical Oncology (Steinkopff Verlag, Darmstadt, 2000)
- <sup>5</sup>M. M. Maisey, R. L. Wahl, and S. E. Barrington, Atlas of Clinical Positron Emission Tomography (Edward Arnold, 1999).
- <sup>6</sup>P. Oehr, H.-J. Biersack, and J. Ruhlmann, *PET in Oncology—Basics and Clinical Applications* (Springer-Verlag, Berlin, 1999).
- <sup>7</sup>R. Carson, M. E. Daube-Witherspoon, and P. Herscovitch, *Quantitative Functional Brain Imaging with Positron Emission Tomography* (Academic, New York, 1998).
- <sup>8</sup>K. Wienhard, R. Wagner, and W.-D. Heiss, *PET—Die Grundlagen und Anwendungen der Positronen-Emissions-Tomographie* (Springer-Verlag, Berlin, 1989).
- <sup>9</sup>J. Radon, "On the determination of functions from their integral values along certain manifolds," translated by P. C. Parks, IEEE Trans. Med. Imaging 5, 170–176 (1986).
- <sup>10</sup>A. C. Melissinos, Experiments in Modern Physics (Academic, San Diego, 1966).
- <sup>11</sup>K. S. Krane, *Introductory Nuclear Physics* (Wiley, New York, 1988).
- <sup>12</sup>G. F. Knoll, Radiation Detection and Measurement (Wiley, New York, 2000), 3rd ed.
- <sup>13</sup>P. Schotanus, G. Stam, E. Gerritse, B. Utts, and B. Briaux, *Crismatec—Scintillation Detectors* (Crismatec, 1992).
- <sup>14</sup>WINTMCA, target systemelectronic, Solingen, Germany, http://www.ggh.de/ target/

### SET OF APPARATUS FOR MAGNETISM AND GALVANISM. PRICE \$52 OR \$70.



Set of Apparatus for Magnetism and Galvanism. Although this apparatus is labelled with the Benjamin Pike name, it was actually made by the Boston firm of Daniel Davis, Jr., or the successor company of Thomas Hall. Three electric engines (18, 19 and 20) are shown. Number 15 is an electromagnet on a stand, number 16 is a galvanoscope for indicating electric current and number 21 is a device for exploding gunpowder electrically. In the lower left-hand corner is an induction coil with a rotating make-and-break contact on its primary. Number 17 is a model of a printing telegraph. (From the 1856 Apparatus Catalogue of Benjamin Pike, Jr. of New York; notes by Thomas B. Greenslade, Jr., Kenyon College)

<sup>&</sup>lt;sup>a)</sup>Electronic mail: kerstin@ikp.tu-darmstadt.de

<sup>&</sup>lt;sup>1</sup>M. A. Mandelkern, "Nuclear techniques for medical imaging: Positron emission tomography," Annu. Rev. Nucl. Part. Sci. **45**, 205–254 (1995).